Desalination and Water Treatment
www.deswater.com

doi:10.5004/dwt.2017.20651

72 (2017) 308–317
April

Adsorption characteristics of graphene oxide in the removal of Cu(II) from aqueous solutions

In-Geol Yi[a], Jin-Kyu Kang[a], Jae-Hyun Kim[b], Seung-Chan Lee[a], Eun-Hye Sim[a], Jeong-Ann Park[b], Song-Bae Kim[a,c,*]

[a]*Environmental Functional Materials and Water Treatment Laboratory, Seoul National University, Korea, Tel. +82-2-880-4587, email: songbkim@snu.ac.kr (S.-B. Kim)*
[b]*Center for Water Resource Cycle Research, Korea Institute of Science and Technology, Seoul 02792, Korea*
[c]*Department of Rural Systems Engineering and Research Institute of Agriculture and Life Sciences, Seoul National University, Korea*

Received 19 September 2016; Accepted 3 March 2017

ABSTRACT

The aim of this study was to investigate the adsorption characteristics of graphene oxide (GO) to remove Cu(II) from aqueous solutions. Batch experiments were performed to examine the effects of adsorbent dose, solution pH, competing Ni(II) ions, reaction time, initial Cu(II) concentration, and temperature on the adsorption of Cu(II) onto GO. Equilibrium, kinetic, and thermodynamic models were used to analyze the sorption data. Fourier-transform infrared (FTIR) and X-ray photoelectron spectroscopy (XPS) analyses were also performed to characterize the adsorption of Cu(II) onto GO. Results showed that the Cu(II) sorption capacity remained relatively constant between pH 3 and 5 (12.26–12.88 mg/g), which was higher than that at pH 2 (5.43 mg/g). In a binary solution of Cu(II) and Ni(II), the Cu(II) sorption capacities (6.61–9.79 mg/g) were higher than those (5.17–7.88 mg/g) of Ni(II). The maximum Cu(II) sorption capacity of GO was determined from the Langmuir isotherm model to be 39.58 mg/g. Sorption model analyses demonstrated that the Langmuir isotherm was best fit to the equilibrium data, whereas the pseudo-first order model was most suitable at describing the kinetic data. Thermodynamic analysis showed that the adsorption of Cu(II) onto GO was endothermic and spontaneous (ΔH° = 0.627 kJ/mol, ΔS° = 2.717 J/K/mol, ΔG° = –0.142 ~ –0.251 kJ/mol). FTIR spectra demonstrated that after the adsorption of Cu(II), the broad band (O=C–OH, carboxyl group) weakened and shifted to 3181 cm^{-1}, whereas the peak at 1164 cm^{-1} (C–OH, hydroxyl group) disappeared . XPS spectra showed that the Cu2p peak appeared in a wide scan of GO after the adsorption of Cu(II). Within a high-resolution scan of the Cu2p region, $Cu2p_{3/2}$ and $Cu2p_{1/2}$ peaks appeared at 932.8 and 953.1 eV, respectively.

Keywords: Adsorption; Copper ions; FTIR; Graphene oxide; XPS

1. Introduction

The contamination of rivers, lakes, and reservoirs by industrial wastewater is a serious environmental problem around the world. Heavy metals are discharged into water bodies, degrading water quality and posing a great threat to human health [1]. Various treatment methods have been applied in the removal of heavy metals from wastewater, including chemical precipitation, coagulation/flocculation, ion exchange, membrane filtration, and adsorption [2]. Among these methods, adsorption is widely applied toward the removal of heavy metals due to its cost-effectiveness and simplicity of operation [3]. Various adsorbents, such as zeolites [4], clays [5], metal oxides [6], agricultural byproducts [7], and chitosan composites [8] have been utilized in the adsorption of heavy metals from wastewater.

Graphene oxide (GO) is a two-dimensional carbonaceous nanomaterial with oxygen-bearing functional groups, such as carbonyl, carboxylic, epoxy, and hydroxyl

*Corresponding author.

groups. Therefore, graphene oxide is hydrophilic and readily dispersed into water [9]. GO has attracted considerable attention within the field of environmental concerns as an adsorbent material. Numerous researchers have used GO as an adsorbent for the removal of heavy metal ions from water and wastewater, demonstrating that GO can effectively bind multi-valent metal ions to the oxygen-containing functional groups on its surface through the formation of a metal complex [10–15]. Copper (Cu) is widely used in metal plating, mining, paint manufacturing, and electronic industries, causing serious health and environmental problems due to a large amount of copper in industrial effluents being released into the environment [16]. Divalent copper (Cu(II)) is known to be both toxic and carcinogenic; the World Health Organization (WHO) has recommended a guideline value of Cu(II) drinking water to be 2.0 mg/L [17].

Recently, GO has been tested by several researchers for the removal of Cu(II) from aqueous solutions [18,19]. These studies can be categorized into two groups based on the type of GO used in the experiments. The first group involves the use of pristine GO toward the removal of Cu(II) from aqueous solutions [20–24], reporting that pristine GO possesses a higher Cu(II) adsorption capacity compared to other carbon-based materials, such as activated carbons and carbon nanotubes. The second type of study is related to modifying GO through the introduction of polymers (calcium alginate, polyvinylpyrrolidone (PVP), chitosan) and other functional materials (2-2′-dipyridylamine, polyaniline, β-cyclodextrin, ethylene diamine tetraacetic acid (EDTA), cadmium sulfide, etc.) into GO for the preparation of GO composites to improve the sorption capacity of Cu(II). The second group has shown that GO composites are high performance adsorbents relative to pristine GO [25–31]. However, GO composites require various types of chemical treatment processing during their preparation, limiting their mass production and large-scale application due to high production costs. Therefore, pristine GO still possesses an advantage over GO composites as an adsorbent for the decontamination of Cu(II). Although several researchers have examined the adsorption of Cu(II) to pristine GO [20–24], more studies are still necessary to improve our understanding of GO with regard to the removal of Cu(II) from aqueous solutions.

The aim of this study was to investigate the adsorption characteristics of GO in the removal of Cu(II) from aqueous solutions. Batch experiments were performed to examine the effects of adsorbent dose, solution pH, competing Ni(II) ions, reaction time, initial Cu(II) concentration, and temperature with regard to the adsorption of Cu(II) onto GO. Equilibrium, kinetic, and thermodynamic models were used to analyze the sorption data. Fourier-transform infrared (FTIR) and X-ray photoelectron spectroscopy (XPS) analyses were also performed to characterize the adsorption of Cu(II) onto GO.

2. Materials and methods

2.1. Graphene oxide

GO (product number: 763705; concentration: 2 mg/mL, dispersion in H_2O) was purchased from Sigma-Aldrich (Saint Louis, MO, USA) and was used without further purification. GO was characterized by various techniques. Field emission scanning electron microscopy (FESEM, Supra 55VP, Carl Zeiss, Oberkochen, Germany) was used to obtain images of GO (Fig. 1a). Transmission electron microscopy (TEM, LIBRA 120, Carl Zeiss, Oberkochen, Germany) was used to analyze

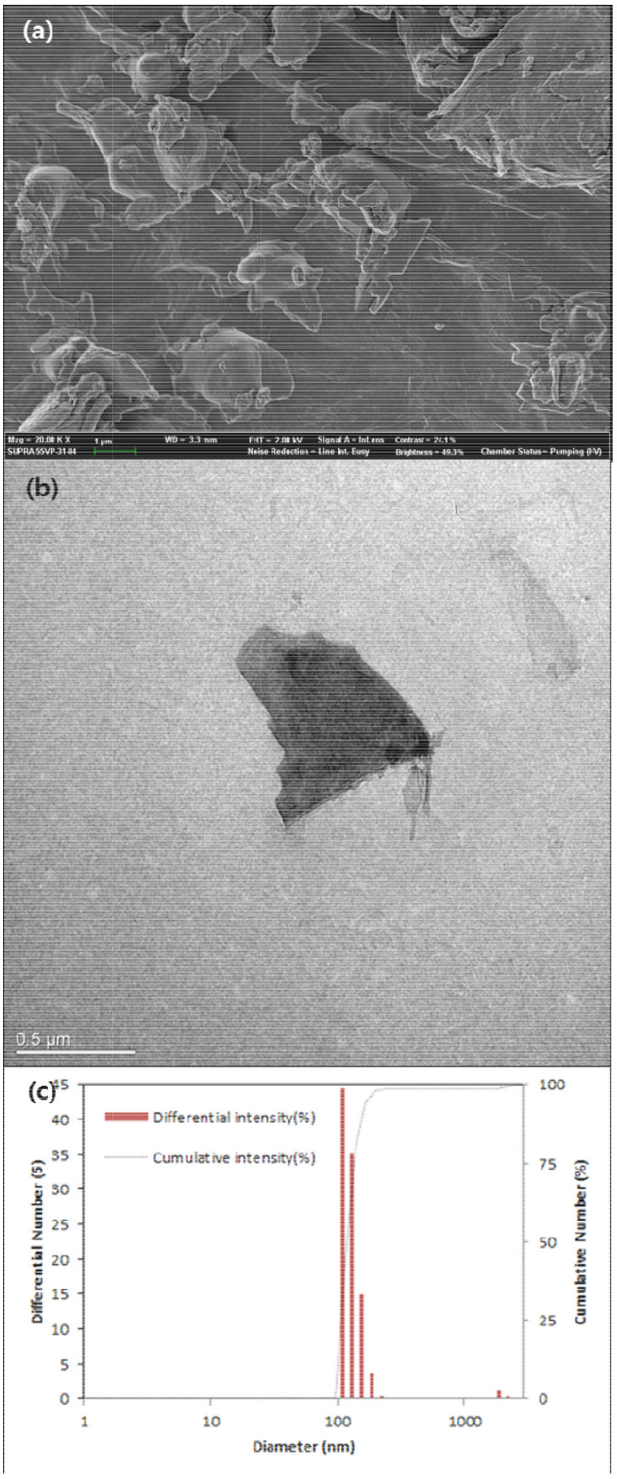

Fig. 1. Characteristics of GO: (a) FESEM image, (b) TEM image, and (c) size distribution.

the surface morphology of GO (Fig. 1b). Also, electrophoretic light scattering (ELS) spectrophotometer (ELS-8000, Otsuka electronics, Osaka, Japan) was used to investigate the size distribution of GO (Fig. 1c, average size = 170.6 ± 278.9 nm). The zeta potential and hydrodynamic diameter of GO in deionized water determined from the ELS measurement were –43.10 mV and 1.17 ± 0.03 μm, respectively [32]. FTIR spectrometer (Nicolet 6700, Thermo Scientific, Waltham, MA, USA) was used to obtain infrared spectra before and after Cu(II) adsorption experiments. XPS (Sigma Probe, Thermo VG, East Grinstead, UK) scans with monochromatic Al Kα radiation were also performed before and after the Cu(II) adsorption experiments.

2.2. Batch experiments

$CuCl_2{\cdot}2H_2O$ was used to prepare stock solutions of Cu(II) (1000 mg/L). Batch experiments were conducted using 15 mL polypropylene conical tubes to examine the adsorption of Cu(II) onto GO. Unless stated otherwise, all experiments were performed in triplicate at a solution pH of 5 and a temperature of 30°C.

The first experiment was performed to observe the effect of the adsorbent (GO) dose on Cu(II) adsorption. The tests were performed at an initial Cu(II) concentration of 25 mg/L with a GO dose of 0.5–1.5 g/L in 6 mL of solution. The tubes were shaken at 150 rpm using a shaking incubator (Daihan Science, Seoul, Korea), and solution samples were collected after reacting for 360 min through centrifugation. The Cu(II) concentrations were analyzed via inductively coupled plasma-atomic emission spectroscopy (ICP-AES) (Optima-4300, PerkinElmer, USA).

The second experiment examined the effect of the solution pH (initial pH = 2–5; initial Cu(II) concentration = 25 mg/L; GO dose = 1 g/L; reaction time = 360 min). A 0.1 M HCl solution was used to adjust the solution pH. Experiments were conducted at pH 2–5 due to the precipitation of Cu(II) ions as $Cu(OH)_2$ at a pH ≥ 6 [33]. The third experiment determined the desorption rate of Cu(II) from the adsorbent. After removal experiments (initial Cu(II) concentration = 25 mg/L; GO dose = 1.5 g/L; reaction time = 360 min; temperature = 30°C), GO was separated from the solution through centrifugation. Then, GO was immersed in a 0.1 M HCl solution and was shaken at 150 rpm for 60 min using a shaking incubator for the desorption of adsorbed Cu(II) ions.

The fourth experiment investigated the effect of the initial Cu(II) concentration (initial Cu(II) concentration = 25–150 mg/L; GO dose = 0.5, 1.0, 2.0 g/L; reaction time = 360 min). For comparison, Ni(II) adsorption experiments were also performed (initial Ni(II) concentration = 25–150 mg L^{-1}; GO dose = 1 g/L; reaction time = 360 min). $Ni(NO_3)_2{\cdot}6H_2O$ was used to prepare stock solutions of Ni(II) (1000 mg/L). Additional experiments were conducted to examine the effect of Ni(II) on the Cu(II) adsorption. Note that Ni(II) is frequently found with Cu(II) in metal plating wastewater [34]. Mixed solutions of Cu(II) and Ni(II) were prepared from Cu(II) and Ni(II) solutions with initial concentrations of 12.5–75 mg/L. After the adsorption experiments (reaction time = 360 min), solution samples were collected via centrifugation. The Cu(II) and Ni(II) concentrations were analyzed by ICP-AES.

The fifth experiment observed the effect of the reaction time onto Cu(II) adsorption (reaction time = 5–720 min; GO dose = 1.0 g/L; initial Cu(II) concentration = 25,75,150 mg/L; temperature = 30°C). After the removal experiments, samples were collected after various reaction times. The final experiment examined the effect of temperature onto Cu(II) adsorption (temperature = 10–50°C; GO dose = 1.0 g/L; initial Cu(II) concentration = 25 mg/L; reaction time = 360 min).

2.3. Adsorption data analysis

The following equations of the determination coefficient (R^2), chi-square coefficient (χ^2), and sum of the absolute error (*SAE*) were used to analyze the adsorption data and confirm the fit to the adsorption model:

$$R^2 = \frac{\sum_{i=1}^{m}\left(y_c - \overline{y_e}\right)_i^2}{\sum_{i=1}^{m}\left(y_c - \overline{y_e}\right)_i^2 + \sum_{i=1}^{m}\left(y_c - y_e\right)_i^2}, \quad (1)$$

$$\chi^2 = \sum_{i=1}^{m}\left[\frac{\left(y_e - y_c\right)^2}{y_c}\right]_i, \quad (2)$$

$$SAE = \sum_{i=1}^{n}\left|y_c - y_e\right|_i, \quad (3)$$

3. Results and discussion

3.1. Cu(II) adsorption onto GO

The Cu(II) adsorption capacity of GO is presented as a function of the adsorbent (GO) dose and solution pH in Fig. 2. As the GO dose increased from 0.5 to 1.5 g/L, the percent removal increased from 37.1 to 60.1%, whereas the adsorption capacity decreased from 18.11 to 9.79 mg/g (Fig. 2a). This result was related to the fact that the adsorption sites available for contaminant removal increased as the adsorbent dose increased. The effect of solution pH on the Cu(II) adsorption by GO is presented in Fig. 2b. The Cu(II) adsorption capacity was 5.43 mg/g at pH 2, and increased sharply to 12.88 mg/g at pH 3. The Cu(II) adsorption capacity remained relatively constant (12.26–12.88 mg/g) between pH 3 and 5. Our results showed that the adsorption capacity at pH 2 was lower than those at pH 3–5. This result could be attributed to a lower dissociation of the oxygen-containing functional groups (higher hydrogen bond formation) on the surface of GO at pH 2 compared to pH 3–5. In addition, higher competition between hydrogen ions and metal ions could occur on the adsorption sites at pH 2 [21]. The point of zero charge (pH_{pzc}) of GO was reported to be 3.8–3.9. At pH 2 (< pH_{pzc}), the surface of GO become more positively-charged relative to pH 3–5, and thus the electrostatic interactions between GO and Cu(II) become less favorable [21]. Similar findings were reported by Sitko et al. [21], who reported that the adsorption of Cu(II) onto GO increased from 55 to 91% as the pH increased from 2 to 3 and remained constant (>90%) at pH 3–5. Ren et al. [22] showed that the removal of Cu(II) by GO increased gradu-

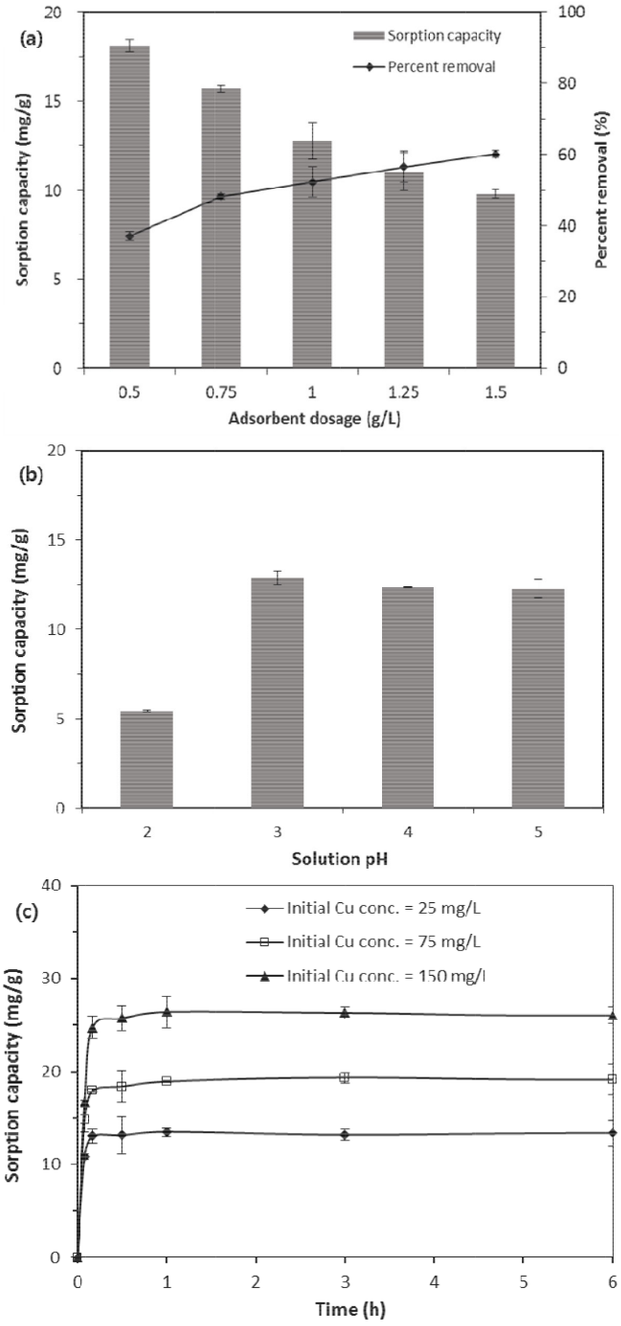

Fig. 2. Cu(II) adsorption onto GO: (a) effect of the adsorbent (GO) dosage, (b) effect of the solution pH, and (c) effect of reaction time.

ally from 19 to 75% by increasing the pH from 3.0 to 5.5. Wu et al. [23] demonstrated that the Cu(II) adsorption capacity of GO increased gradually from 10.75 to 39 mg/g with a rise in pH from 1.0 to 5.3 (initial Cu(II) concentration = 50 mg/L). The effect of reaction time on the Cu(II) adsorption by GO is presented in Fig. 2c. The adsorption of Cu(II) onto GO was a fast process, reaching equilibrium within 15 min in the initial Cu(II) concentrations of 25–150 mg/L. Note that kinetic sorption model analysis was not performed because only three data points could be used to simulate the adsorption rate because the other points reached equilibrium.

The adsorption-desorption experimental results are presented in Table 1. The quantity of Cu(II) adsorbed onto GO was 9.86 mg/g under the given experimental conditions (initial Cu(II) concentration = 25 mg/L, GO dose = 1.5 g/L). After treatment with a solution of 0.1 M HCl, the Cu(II) desorbed from GO was 9.48 mg/g with a desorption rate of 96.11%. Wu et al. [23] showed that the desorption rate of Cu(II) from GO increased from 1 to 74% as the pH decreased from 5.7 to 1.0, which was adjusted by a solution of HCl during the desorption experiments. They also reported that the Cu(II) adsorption capacity of GO still remained at >90% of its initial capacity after ten adsorption-desorption cycles, demonstrating that GO could be repeatedly used for the removal of Cu(II) via adsorption-desorption procedures. In addition, the reusability of GO-based adsorbents with regard to the removal of Cu(II) has been reported for a GO-Fe_3O_4 composite [18] and GO-(2,2′-dipyridylamine) composite [30].

The Cu(II) adsorption onto GO in the absence and presence of competing Ni(II) ions is presented in Fig. 3. In a single solution of Cu(II), the adsorption capacity of GO increased from 13.06 to 24.01 mg/g as the initial Cu(II) concentration increased from 25 to 150 mg/L. In a single solution of Ni(II), the adsorption capacity increased from 8.23 to 14.24 mg/g by increasing the initial Ni(II) concentration from 25 to 150 mg/L. Our results demonstrated that the removal of Cu(II) by GO was higher than the removal of Ni(II) in a single solution. Similar findings were reported by

Table 1
Adsorption–desorption experiment for Cu(II) on GO

Initial Cu(II) conc. (mg/L)	25.0
GO dose (g/L)	1.5
Cu(II) adsorbed (mg/g)	9.86
Cu(II) desorbed (mg/g)	9.48
Desorption rate (%)	96.11

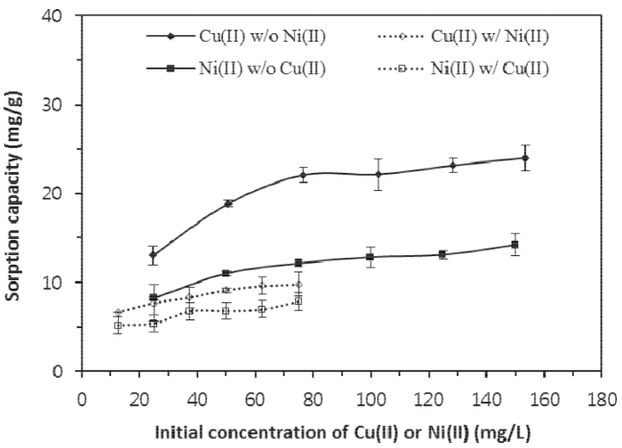

Fig. 3. Cu(II) adsorption onto GO in the absence and presence of competing Ni(II) ions.

Zare-Dorabei et al. [30] who performed the Cu(II) and Ni(II) adsorption tests in a single solution using a GO-(2,2′-dipyridylamine) composite as the adsorbent. The authors demonstrated that the Langmuir adsorption of Cu(II) was 358.824 mg/g, which was higher than that (180.893 mg/g) of Ni(II). In a binary solution of Cu(II) and Ni(II), the Cu(II) adsorption capacities (6.61–9.79 mg/g) were higher than those (5.17–7.88 mg/g) of Ni(II), demonstrating a higher binding affinity of Cu(II) to the adsorption sites of GO compared to Ni(II). Our results also showed that for the same initial Cu(II) concentrations (25, 50, and 75 mg/L), the adsorption capacities of Cu(II) in the presence of Ni(II) were lower than those of Cu(II) in the absence of Ni(II), due to the competitive binding of Ni(II) in the binary solution.

3.2. Equilibrium data analysis

Adsorption data obtained from batch tests as a function of the initial Cu(II) concentration were analyzed using the following equilibrium isotherm models [35]:

$$q_e = \frac{Q_m K_L C_e}{1 + K_L C_e} \quad \text{Langmuir} \quad (4)$$

$$q_e = K_F C_e^{\frac{1}{n}} \quad \text{Freundlich} \quad (5)$$

$$q_e = \frac{RT}{b_T} \ln A_T C_e \quad \text{Temkin} \quad (6)$$

$$q_e = \frac{K_R C_e}{1 + a_R C_e^{\ g}} \quad \text{Redlich-Peterson} \quad (7)$$

The observed data and applied equilibrium models are presented in Fig. 4. The corresponding model parameters are provided in Table 2. The values of R^2, χ^2, and SAE indicated that the Langmuir isotherm exhibited the best fit to the equilibrium data. The Langmuir model assumes monolayer adsorption on finite and homogeneous adsorption sites on the adsorbents [33]. From the Langmuir model, the following parameter values were determined: Q_m = 12.69–39.58 mg/g and K_L = 0.055–0.115 L/mg (Table 2). As the adsorbent (GO) dosage increased from 0.5 to 2.0 g/L, the value of Q_m (maximum adsorption capacity) decreased, whereas the value of K_L (affinity of binding sites) increased due to an increase in adsorption sites. A dimensionless separation factor (R_L) was calculated using the following relationship:

$$R_L = \frac{1}{1 + K_L C_0} \quad (8)$$

The values of R_L were calculated to be 0.054–0.108, indicating that the adsorption of Cu(II) onto GO was highly favorable [33]. Under the given experimental conditions (GO dose = 0.5 g/L, initial Cu(II) concentration = 25–150 mg/L, reaction time = 360 min, temperature = 30°C), the maximum Cu(II) adsorption capacity of GO was determined to be 39.58 mg/g. Our value was within the range of the Cu(II) adsorption capacity for GO (21.49–294 mg/g) reported in the literature (Table 3). Discrepancies between our value and the values reported in the literature could be attributed to differences in the experimental conditions used in the tests, including the initial Cu(II) concentration, GO dose, solution pH, and ionic strength. Numerous researchers have used carbon-based nanomaterials such as single-walled and multi-walled nanotubes (CNTs) for the removal of heavy metal ions from aqueous solutions [36–40]. According to the literature survey

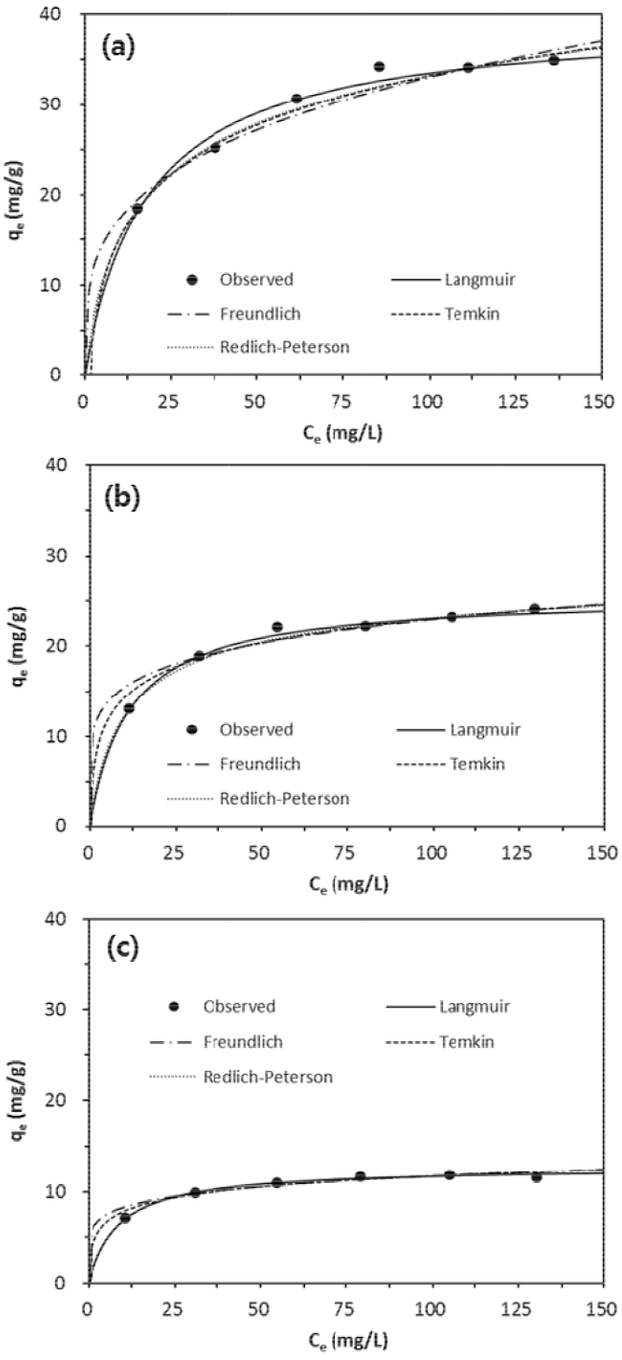

Fig. 4. Equilibrium isotherm model analysis with the Langmuir, Freundlich, and Redlich-Peterson models. Model parameters are provided in Table 2.

Table 2
Equilibrium model parameters obtained from the experimental data

Adsorbent dose	0.5 g/L	1.0 g/L	2.0 g/L
Langmuir			
Q_m (mg/g)	39.58	25.65	12.69
K_L (L/mg)	0.055	0.088	0.115
R^2	0.978	0.990	0.990
χ^2	0.169	0.045	0.015
SAE	3.390	1.701	0.764
Freundlich			
K_F (L/g)	9.03	10.38	5.80
1/n	0.282	0.172	0.153
R^2	0.955	0.936	0.913
χ^2	0.401	0.583	0.252
SAE	6.501	4.194	2.542
Temkin			
A_T (L/g)	0.605	4.274	9.546
b_T (J/mol)	318.54	663.14	1476.01
R^2	0.972	0.960	0.940
χ^2	0.218	0.306	0.142
SAE	4.502	3.436	2.143
Redlich-Peterson			
K_R (L/g)	3.501	2.911	1.495
a_R (L/mg)	0.187	0.164	0.120
K_R/a_R (mg/g)	18.76	17.73	12.48
g	0.854	0.924	0.997
R^2	0.974	0.982	0.990
χ^2	0.195	0.081	0.016
SAE	4.328	2.040	0.740

[41–44], the maximum Cu(II) adsorption capacity of CNTs was determined to be 1.33–43.16 mg/g, indicating that the Cu(II) adsorption capacity of GO (21.49–294 mg/g) is much higher that of CNTs.

3.3. Thermodynamic data analysis

The adsorption data were analyzed to determine the effect of temperature on the adsorption of Cu(II) onto GO using the following relationships [45]:

$$\Delta G^0 = \Delta H^0 - T\Delta S^0 \tag{9}$$

$$\Delta G^0 = -RT\ln K_e \tag{10}$$

$$\ln\left(K_e\right) = \frac{\Delta S^0}{R} - \frac{\Delta H^0}{RT}; K_e = \frac{aq_e}{C_e} \tag{11}$$

The observed data and applied thermodynamic model are presented in Fig. 5, whereas the related model parameters are presented in Table 4. The value of ΔH° was determined to be 0.627 kJ/mol, indicating that the adsorption of Cu(II) onto GO was endothermic and increased with a rise in temperature. The value of ΔS° was 2.717 J/K/mol, suggesting that randomness increased at the interface between the Cu(II) solution and GO surface during the adsorption process. The values of ΔG° were determined to be negative (–0.142 ~ –0.251 kJ/mol), indicating that the adsorption of Cu(II) onto GO was a spontaneous process. Our results were in good agreement with those of reports from other

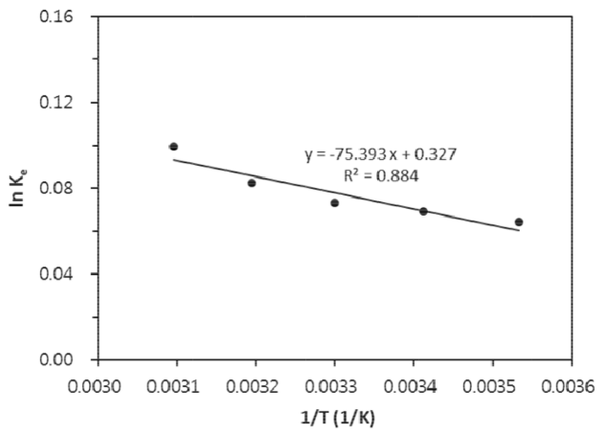

Fig. 5. Thermodynamic model analysis. Model parameters are provided in Table 4.

Table 3
Maximum Cu(II) adsorption capacity of pristine GO from the Langmuir isotherm reported in the literature

Adsorption capacity (mg/g)	Initial Cu(II) concentration (mg/L)	GO dose (g/L)	Solution condition	Reference
21.49	–	0.4	IS = 0.01 M $NaNO_3$, pH = 5.3	[18]
46.6	3.2–63.5	0.5	pH = 5	[20]
294	–	0.1	pH = 5	[21]
74.98	–	0.1	IS = 0.01 M, pH = 5	[22]
117.5	25–250	1.0	pH = 5.3	[23]
73.36	6.4–158.9	–	IS = 0.01 M $NaNO_3$, pH = 5	[24]
39.58	25–150	0.5	pH = 5	This study

IS = ionic strength

Table 4
Thermodynamic parameters obtained from the experimental data

Temp. (°C)	ΔH° (kJ/mol)	ΔS° (J/K mol)	ΔG° (kJ/mol)
10	0.627	2.717	−0.142
20			−0.169
30			−0.196
40			−0.224
50			−0.251

researchers who demonstrated the endothermic nature of Cu(II) adsorption onto GO-based adsorbents, including GO-Fe_3O_4 composites [18], GO aerogels [19], GO-chitosan aerogels [25], chitosan/sulfydryl-functionalized GO composites [13], and GO-cadmium sulfide composites [29]. For instance, Li et al. [18] reported that the adsorption of Cu(II) onto GO-Fe_3O_4 composites increased from 18.26 to 25.57 mg/g as the temperature increased from 20 to 40°C. Mi et al. [19] also reported that the Langmuir Cu(II) adsorption capacity of GO aerogel increased from 17.73 to 29.59 g/g with a rise in temperature from 10 to 40°C.

3.4. FTIR and XPS analyses

The FTIR spectra of GO before and after the Cu(II) adsorption experiments are presented in Fig. 6. In the FTIR spectrum for Cu(II) prior to adsorption, a broad band at 3205 cm^{-1} was assigned to the stretching vibrations of –COOH and –OH groups. The peak at 1723 cm^{-1} was attributed to the C=O bond from the carboxyl group. The peak at 1618 cm^{-1} was ascribed to the C=C bonds found in benzene rings, whereas the peak at 1164 cm^{-1} was attributed to the O–H stretching from phenolic groups. The peak at 1035 cm^{-1} was assigned to the C–O stretching from the carboxyl group [10,20,22,46]. In the FTIR spectrum for Cu(II) after adsorption, changes were detected at 3205 cm^{-1} and 1164 cm^{-1}, due to complexation of Cu(II) ions with adsorption sites. The broad band at 3205 cm^{-1} weakened and shifted to 3181 cm^{-1}, whereas the peak at 1164 cm^{-1} disappeared [10].

The XPS spectra of GO before and after the Cu(II) adsorption experiments can be seen in Fig. 7. In a wide

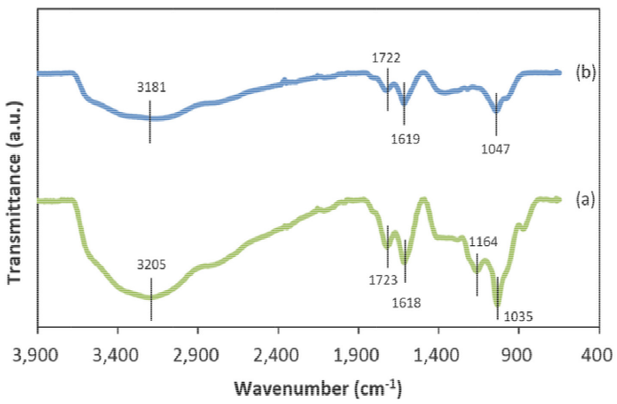

Fig. 6. FTIR spectra of GO (a) before and (b) after Cu(II) sorption experiments.

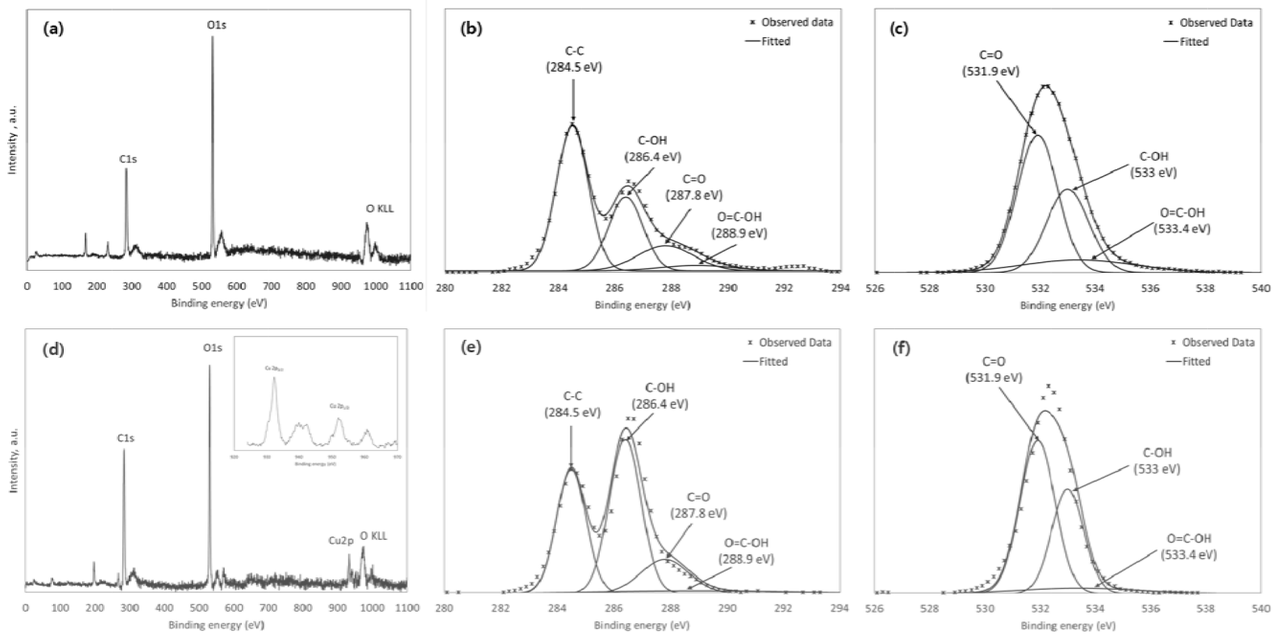

Fig. 7. XPS spectra of GO before and after Cu(II) sorption experiments: (a) wide scan prior to sorption; (b) high resolution scan of the C1s region prior to sorption; (c) high resolution scan of the O1s region prior to sorption; (d) wide scan after sorption (inset = high-resolution scan of the Cu2p region); (e) high resolution scan of the C1s region after sorption; (c) high resolution scan of the O1s region after sorption.

scan of GO before Cu(II) adsorption (Fig. 7a), the photoelectron peaks at binding energies of 285 and 531 eV were attributed to C1s and O1s, respectively. After the adsorption of Cu(II), the Cu2p peak at a binding energy of 932 eV appeared in a wide scan of GO (Fig. 7d). Within a high-resolution scan of the Cu2p region (inset of Fig. 7d), $Cu2p_{3/2}$ and $Cu2p_{1/2}$ peaks appeared at 932.8 and 953.1 eV, respectively, whereas satellite peaks could be found at the higher binding energy sides [47]. These results were in good agreement with the standard spectrum for CuO [47,48]. In the C1s spectrum (Fig. 7b and 7e), the peak at 284.5 eV was assigned to C=C, which were contributed from the structure of graphite. Other peaks at 286.4, 287.8, and 288.9 eV were assigned to C–OH (hydroxyl group), C=O (carbonyl group), and O=C–OH (carboxyl group), respectively, which were carbon atoms bound to oxygen-containing moieties [49]. Within the O1s spectrum (Fig. 7c and 7f), the peaks at 531.9, 533.0, and 533.4 eV could be attributed to C=O, C–OH, and O=C–OH, respectively [349]. Our results indicated that oxygen-containing functional groups on the surface of GO were involved in the adsorption of Cu(II) ions.

4. Conclusions

The adsorption characteristics of graphene oxide (GO) with regard to the removal of Cu(II) from aqueous solutions were investigated. Batch experiments showed that the Cu(II) adsorption capacity remained relatively constant between pH 3 and 5, which was higher than the capacity measured at pH 2. In a binary solution of Cu(II) and Ni(II), the adsorption capacity of Cu(II) was higher than that of Ni(II). The maximum Cu(II) adsorption capacity of GO was determined to be 39.58 mg/g. Adsorption model analyses demonstrated that the Langmuir isotherm model was best fit to the equilibrium data, whereas the pseudo-first order model was most suitable at describing the kinetic data. Thermodynamic analysis showed that the adsorption of Cu(II) onto GO was endothermic and spontaneous. FTIR spectra demonstrated that oxygen-containing functional groups (hydroxyl, carbonyl, and carboxyl groups) on the surface of GO were involved in the adsorption of Cu(II). XPS spectra showed that the Cu2p peak appeared in a wide scan of GO after the adsorption of Cu(II). Further experiments are necessary using metal-laden wastewater with various ionic composition/strength and complexing agents in order to evaluate the applicability of GO as adsorbents for heavy metal ions. In addition, the adsorption capacity and cost-effectiveness of GO should be compared with other adsorbents for potential application to industrial wastewater.

Acknowledgments

This work was supported by the National Research Foundation of Korea, funded by the Ministry of Education, Republic of Korea (grant number 2015–059565).

Symbols

a	—	Adsorbent dose
a_R	—	Redlich-Peterson constant
A_T	—	Temkin isotherm constant related to adsorption capacity
b_T	—	Temkin isotherm constant related to adsorption intensity
C_e	—	Equilibrium concentration of solute in the aqueous solution
g	—	Redlich-Peterson isotherm exponent
K_F	—	Freundlich constant related to adsorption capacity
K_L	—	Langmuir constant related to the affinity of binding sites
K_R	—	Redlich-Peterson constant
K_e	—	Equilibrium constant (dimensionless)
$1/n$	—	Freundlich constant related to adsorption intensity
Q_m	—	Langmuir maximum adsorption capacity
q_e	—	Amount of solute adsorbed at equilibrium
R	—	Gas constant
R^2	—	Determination coefficient
R_L	—	Separation factor
SAE	—	Sum of absolute error
T	—	Temperature (K)
y_c	—	Calculated removal capacity from the model
y_e	—	Measured removal capacity from the experiment,
y_{e^-}	—	Average of the measured removal capacity
χ^2	—	Chi-square coefficient
ΔG^0	—	Change in Gibb's free energy
ΔH^0	—	Change in enthalpy
ΔS^0	—	Change in entropy

References

[1] J.K. Ahmed, M. Ahmaruzzaman, A review on potential usage of industrial waste materials for binding heavy metal ions from aqueous solutions, J. Water Proc. Eng., 10 (2016) 39–47.
[2] F. Fu, Q. Wang, Removal of heavy metal ions from wastewaters: A review, J. Environ Manage., 92 (2011) 407–418.
[3] S. Babel, T.A. Kurniawan, Low-cost adsorbents for heavy metals uptake from contaminated water: a review, J. Hazard. Mater., B97 (2003) 219–243.
[4] S. Wang, Y. Peng, Natural zeolites as effective adsorbents in water and wastewater treatment, Chem. Eng. J., 156 (2010) 11–24.
[5] K.G. Bhattacharyya, S.S. Gupta, Adsorption of a few heavy metals on natural and modified kaolinite and montmorillonite: A review, Adv. Colloid Interf. Sci., 140 (2008) 114–131.
[6] M. Hua, S. Zhang, B. Pan, W. Zhang, L. Lv, Q. Zhang, Heavy metal removal from water/wastewater by nanosized metal oxides: A review, J. Hazard. Mater., 211–212 (2012) 317–331.
[7] T.A.H. Nguyen, H.H. Ngo, W.S. Guo, J. Zhang, S. Liang, Q.Y. Yue, Q. Li, T.V. Nguyen, Applicability of agricultural waste and by-products for adsorptive removal of heavy metals from wastewater, Bioresour. Technol., 148 (2013) 574–585.
[8] W.S.W. Ngah, L.C. Teong, M.A.K.M. Hanafiah, Adsorption of dyes and heavy metal ions by chitosan composites: A review, Carbohyd. Polym., 83 (2011) 1446–1456.
[9] D.R. Dreyer, S. Park, C.W. Bielawski, R.S. Ruoff, The chemistry of graphene oxide. Chem. Soc. Rev., 39 (2010) 228–240.

[10] Y. Ren, N. Yan, J. Feng, J. Mab, Q. Wen, N. Li, Q. Dong, Adsorption mechanism of copper and lead ions onto graphene nanosheet/δ-MnO_2, Mater. Chem. Phys., 136 (2012) 538–544.
[11] L. Li, C. Luo, X. Li, H. Duan, X. Wang, Preparation of magnetic ionic liquid/chitosan/graphene oxide composite and application for water treatment, Int. J. Biol. Macromol., 66 (2014) 172–178.
[12] X. Guo, B. Du, Q. Wei, J. Yang, L. Hu, L. Yan, W. Xu, Synthesis of amino functionalized magnetic graphenes composite material and its application to remove Cr(VI), Pb(II), Hg(II), Cd(II) and Ni(II) from contaminated water, J. Hazard. Mater., 278 (2014) 211–220.
[13] X. Li, H. Zhou, W. Wu, S. Wei, Y. Xu, Y. Kuang, Studies of heavy metal ion adsorption on chitosan/sulfydryl-functionalized graphene oxide composites, J Colloid. Interf. Sci., 448 (2015) 389–397.
[14] X. Wang, Z. Chen, S. Yang, Application of graphene oxides for the removal of Pb(II) ions from aqueous solutions: Experimental and DFT calculation, J. Mol. Liquid., 211 (2015) 957–964.
[15] L. Cui, Y. Wang, L. Gao, L. Hu, L. Yan, Q. Wei, B. Du, EDTA functionalized magnetic graphene oxide for removal of Pb(II), Hg(II) and Cu(II) in water treatment: Adsorption mechanism and separation property, Chem. Eng. J., 281 (2015) 1–10.
[16] A. Agrawal, S. Kumari, K. Sahu, Iron and copper recovery/removal from industrial wastes: a review, Ind. Eng. Chem. Res., 48 (2009) 6145–6161.
[17] World Health Organization (WHO), Guidelines for drinking-water quality, 4th ed., WHO, Geneva, 2011.
[18] J. Li, S. Zhang, C. Chen, G. Zhao, X. Yang, J. Li, X. Wang, Removal of Cu(II) and fulvic acid by graphene oxide nanosheets decorated with Fe_3O_4 nanoparticles, Appl. Mater. Interf., 4 (2012) 4991–5000.
[19] X. Mi, G. Huang, W. Xie, W. Wang, Y. Liu, J. Gao, Preparation of graphene oxide aerogel and its adsorption for Cu^{2+} ions, Carbon, 50 (2012) 4856–4864.
[20] S.T. Yang, Y. Chang, H. Wang, G. Liu, S. Chen, Y. Wang, Y. Liu, A. Cao, Folding/aggregation of graphene oxide and its application in Cu^{2+} removal, J. Colloid Interf. Sci., 351 (2010) 122–127.
[21] R. Sitko, E. Turek, B. Zawisza, E. Malicka, E. Talik, J. Heimann, A. Gagor, B. Feist, R. Wrzalik, Dalton Trans., 42 (2013) 5682–5689.
[22] X. Ren, J. Li, X. Tan, X. Wang, Comparative study of graphene oxide, activated carbon and carbon nanotubes as adsorbents for copper decontamination, Dalton Trans., 42 (2013) 5266–5274.
[23] W. Wu, Y. Yang, H. Zhou, T. Ye, Z. Huang, R. Liu, Y. Kuang, Highly efficient removal of Cu(II) from aqueous solution by using graphene oxide, Water Air Soil Pollut., 224 (2013) 1372–1379.
[24] S. Yang, L. Li, Z. Pei, C. Li, X. Shan, B. Wen, S. Zhang, L. Zheng, J. Zhang, Y. Xie, R. Huang, Effects of humic acid on copper adsorption onto few-layer reduced graphene oxide and few-layer graphene oxide, Carbon., 75 (2014) 227–235.
[25] B. Yu, J. Xu, J.H. Liu, S.T. Yang, J. Luo, Q. Zhou, J. Wan, R. Liao, H. Wang, Y. Liu, Adsorption behavior of copper ions on graphene oxide–chitosan aerogel, J. Environ. Chem. Eng., 1 (2013) 1044–1050.
[26] W.M. Algothmi, N.M. Bandaru, Y. Yu, J.G. Shapter, A.V. Ellis, Alginate–graphene oxide hybrid gel beads: an efficient copper adsorbent material, J. Colloid Interf. Sci., 397 (2013) 32–38.
[27] X. Hu, Y. Liu, H. Wang, A. Chen, G. Zeng, S. Liu, Y. Guo, X. Hu, T. Li, Y. Wang, L. Zhou, S. Liu, Removal of Cu(II) ions from aqueous solution using sulfonated magnetic graphene oxide composite, Sep. Purif. Technol., 108 (2013) 189–195.
[28] X. Hu, Y. Liu, H. Wang, G. Zeng, X. Hu, Y. Guo, T. Li, A. Chen, L. Jiang, F. Guo, Adsorption of copper by magnetic graphene oxide-supported β-cyclodextrin: Effects of pH, ionic strength, background electrolytes, and citric acid, Chem. Eng. Res. Design., 93 (2015) 675–683.
[29] T. Jiang, W. Liu, Y. Mao, L. Zhang, J. Cheng, M. Gong, H. Zhao, L. Dai, S. Zhang, Q. Zhao, Adsorption behavior of copper ions from aqueous solution onto graphene oxide–CdS composite, Chem. Eng. J., 259 (2015) 603–610.
[30] R. Zare-Dorabei, S.M. Ferdowsi, A. Barzin, A. Tadjarodi, Highly efficient simultaneous ultrasonic-assisted adsorption of Pb(II), Cd(II), Ni(II) and Cu (II) ions from aqueous solutions by graphene oxide modified with 2,2′-dipyridylamine: central composite design optimization, Ultrason. Sonochem., 32 (2016) 265–276.
[31] Y. Liu, L. Chen, Y. Li, P. Wang, Y. Dong, Synthesis of magnetic polyaniline/graphene oxide composites and their application in the efficient removal of Cu(II) from aqueous solutions, J. Environ. Chem. Eng., 4 (2016) 825–834.
[32] J.K. Kang, J.A. Park, I.G. Yi, S.B. Kim, Experimental and modeling analyses for interactions between graphene oxide and quartz sand. J. Environ. Sci. Heal. A. (2017) published online.
[33] N. Ferrah, O. Abderrahim, M.A. Didi, D. Villemin, Removal of copper ions from aqueous solutions by a new sorbent: Polyethyleneiminemethylene phosphonic acid. Desalination, 269 (2011) 17–24.
[34] C.G. Lee, S. Lee, J.A. Park, C. Park, S.J. Lee, S.B. Kim, B. An, S.T. Yun, S.H. Lee, J.W. Choi, Removal of copper, nickel and chromium mixtures from metal plating wastewater by adsorption with modified carbon foam, Chemosphere, 166 (2017) 203–211.
[35] K.Y. Foo, B.H. Hameed, Insights into the modeling of adsorption isotherm systems, Chem. Eng. J., 156 (2010) 2–10.
[36] Ihsanullah, A. Abbas, A.M. Al-Amer, T. Laoui, M.J. Al-Marri, M.S. Nasser M. Khraisheh, M.A. Atieh, Heavy metal removal from aqueous solution by advanced carbon nanotubes: Critical review of adsorption applications, Sep. Purif. Technol., 157 (2016) 141–161.
[37] V.K. Gupta, O. Moradi, I. Tyagi, S. Agarwal, H. Sadegh, R. Shahryari-Ghoshekandi, A.S.H. Makhlouf, M. Goodarzi, A. Garshasbi, Study on the removal of heavy metal ions from industry waste by carbon nanotubes: effect of the surface modification-A review, Crit. Rev. Environ. Sci. Technol., 46 (2016) 93–118.
[38] O. Moradi, K. Zare, M. Monajjemi, M. Yari, H. Aghaie, The studies of equilibrium and thermodynamic adsorption of Pb(II), Cd(II) and Cu(II) ions from aqueous solution onto SWCNTs and SWCNT–COOH surfaces, Fullerene. Nanotube. Carbon Nanostruc., 18 (2010) 285–302.
[39] O. Moradi, K. Zare, Adsorption of Pb(II), Cd(II) and Cu(II) ions from aqueous solution onto SWCNTs and SWCNT–COOH surfaces: Kinetics study, Fullerene. Nanotube. Carbon Nanostruc., 19 (2010) 628–652.
[40] O. Moradi, M. Yari, K. Zare, B. Mirza, F. Najafi, Carbon nanotubes: A review of chemistry principles and reactions, Fullerene. Nanotube. Carbon Nanostruc., 20 (2012) 138–151.
[41] Y.H. Li, Z. Luan, X. Xiao, X. Zhou, C. Xu, D. Wu, B. Wei, Removal of Cu^{2+} ions from aqueous solutions by carbon nanotubes, Adsorp. Sci. Technol., 21 (2003) 475–485.
[42] J. Wang, Z. Li, S. Li, W. Qi, P. Liu, F. Liu, Y. Ye, L. Wu, L. Wang, W. Wu, Adsorption of Cu(II) on oxidized multi-walled carbon nanotubes in the presence of hydroxylated and carboxylated fullerenes, Plos One, 8 (2013) e72475.
[43] Y. Ge, Z. Li, D. Xiao, P. Xiong, N. Ye, Sulfonated multi-walled carbon nanotubes for the removal of copper (II) from aqueous solutions, J. Indust. Eng. Chem., 20 (2014) 1765–1771.
[44] A. Sadeghinya, B. Bina, A.H. Mahvi, A. Esrafili, E. Dehghanifard, L.K. Takanlu, Efficiency determination of single-walled carbon nanotubes on adsorption of copper ions from synthetic wastewater, Intern. J. Environ. Heal. Eng., 4 (2015) 1–6.
[45] S.Y. Yoon, C.G. Lee, J.A. Park, J.H. Kim, S.B. Kim, S.H. Lee, J.W. Choi, Kinetic, equilibrium and thermodynamic studies for phosphate adsorption to magnetic iron oxide nanoparticles, Chem. Eng. J., 236 (2014) 341–347.

[46] H. Zhang, D. Hines, D.L. Akins, Synthesis of a nanocomposite composed of reduced graphene oxide and gold nanoparticles, Dalton Trans., 43 (2014) 2670–2675.
[47] D. Gao, G. Yang, J. Li, J. Zhang, J. Zhang, D. Xue, Room-temperature ferromagnetism of flower like CuO nanostructures, J. Phys. Chem., C 114 (2010) 18347–18351.
[48] A. Pendashteh, M.F. Mousavi, M.S. Rahmanifar, Fabrication of anchored copper oxide nanoparticles on graphene oxide nanosheets via an electrostatic coprecipitation and its application as supercapacitor, Electrochim. Acta., 88 (2013) 347–357.
[49] D. Yang, A. Velamakanni, G. Bozoklu, S. Park, M. Stoller, R.D. Piner, S. Stankovich, I. Jung, D.A. Field, C.A. Ventrice Jr, R.S. Ruoff, Chemical analysis of graphene oxide films after heat and chemical treatments by X-ray photoelectron and Micro-Raman spectroscopy, Carbon, 47 (2009) 145–152.